Eur Biophys J (2000) 29: 420–428

ARTICLE

Chris Walters · Anthony Clarke · Matthew J. Cliff
Peter A. Lund · Stephen E. Harding

Trp203 mutation in GroEL promotes a self-association reaction: a hydrodynamic study

Received: 4 January 2000 / Revised version: 5 April 2000 / Accepted: 5 April 2000

Abstract A combination of sedimentation equilibrium and sedimentation velocity in the analytical ultracentrifuge is used to investigate the hydrodynamic integrity and increased self-association interactions of the mutant GroEL Y203W when compared to the wild-type GroEL molecule, which may be derived from increased hydrophobic exposure caused by the mutation. Sedimentation velocity has revealed that three distinct species were present throughout the concentration ranges used, corresponding to 14-mer (GroEL ''super monomer'') and 28-mer (''super dimer'') subunit compositions with a small amount of 42-mer (''super trimer''), which, from the relative concentration of each species, would give an estimated weight average molecular weight of $(1.0 \pm 0.1) \times 10^6$ Da. Sedimentation equilibrium gave an apparent weight average molecular weight ($M_{w,app}$) of (910,000 ± 5000) Da, which is in agreement with these findings. These results are in contrast to wild-type GroEL which, in excellent agreement with the previous findings of Behlke and co-workers, revealed a single species with an $M_{w,app}$ of (805,000 ± 5200) Da and a sedimentation coefficient $s^0_{20,w}$ of (21.6 ± 0.3) S. We therefore conclude that the tryptophan mutation at the Y203 location causes a significant degree of self-association of the GroEL 14-mer assembly (with dimer and trimer present). These findings would appear to correlate well with the findings of Gibbons et al., who showed an increase in hydrophobic exposure due to this mutation.

C. Walters · S.E. Harding (✉)
National Centre for Macromolecular Hydrodynamics,
University of Nottingham, School of Biological Sciences,
Sutton Bonington, Leics. LE12 5RD, UK
e-mail: steve.harding@nottingham.ac.uk

A. Clarke · M.J. Cliff
University of Bristol, Department of Biochemistry,
Tyndall Avenue, Bristol BS8 1TD, UK

P.A. Lund
University of Birmingham, School of Biosciences,
Birmingham B15-2TT, UK

Key words GroEL · Chaperonin · Ultracentrifugation · Sedimentation equilibrium · Sedimentation velocity

Introduction

The *Escherichia coli* chaperonin system GroEL and GroES has to date been the most widely studied of the chaperonin proteins. Together they have been shown to facilitate the folding and assembly of many proteins in *E. coli* (Behlke et al. 1997; Gibbons et al. 1996; Saibil et al. 1993) and have been implicated in the transport of nascent polypeptides in vivo (Gething and Sambrook 1992). The GroEL system is also known to be part of a class of ''cpn60'' proteins found in mitochondria, chloroplasts and prokaryotic cells (Hemmingsen et al. 1988), where ''cpn'' means ''chaperonin'' and ''60'' means the monomeric protein unit has an approximate molecular weight of 60 kDa (by contrast, GroES is a class of cpn10 protein).

From X-ray diffraction studies (Braig et al. 1994), in the crystallised state, GroEL appears to consist of 14 identical monomers with molecular weights M_w of 57,138 Da each (from amino acid content). These subunits are arranged in two stacked heptameric rings to give a seven-fold symmetrical cylindrical complex. Each subunit consists of around 547 amino acid residues folded into three domains: an apical domain consisting of residues 191–376, an intermediate domain consisting of residues 134–190 and 377–408 and an equatorial domain consisting of residues 6–133 and 409–523. Electron microscopy studies of GroEL in the cryo-prepared state (Langer et al. 1992; Chen et al. 1994; Saibil 1994) have suggested that polypeptides requiring folding are bound in the central cavity of GroEL. Such studies have identified a set of hydrophobic residues on the apical domain lining the channel, which provides the binding surface for exposed hydrophobic regions of substrate proteins. These regions are apparently close to the surface of the cylinder and are facing inwards, which

is thought to prevent self-aggregation of the GroEL (Saibil 1994). More recent studies (Brazil et al. 1998) have shown that binding of divalent cations such as Zn^{2+} and Mg^{2+} to the equatorial domain leads to an increased exposure of these hydrophobic regions, which in turn increases the potential for substrate protein-GroEL interaction. It is also known that replacement of the tyrosine residue (Y203) in the apical region with a non-hydrophobic glutamate (E203) causes a total loss of substrate protein binding to the GroEL molecule and disrupts the binding of the co-chaperonin GroES (Fenton et al. 1994); such disruption is likely to be caused by a combination of a small conformation change in the GroEL binding regions and reduced hydrophobic interactions with substrate proteins. Furthermore, fluorescence studies on a GroEL mutant containing a single tyrosine to tryptophan replacement (Y203W) have indicated some increased hydrophobic exposure in the apical domain region of the molecule (Gibbons et al. 1996). This again reinforces the suggestion that this point mutation may cause a conformational change that leads to the increased exposure of the hydrophobic binding regions normally found less exposed facing the inward binding cavity (Fig. 1).

It would therefore be highly instructive to investigate the oligomeric composition of the Trp mutant of *E. coli* cpn 60 (GroEL Y203W). In this study we have done this by using a combination of sedimentation equilibrium and sedimentation velocity in the analytical ultracentrifuge to determine the hydrodynamic stability and possible further self-association interactions of the molecule due to increased hydrophobic exposure that may be caused by the mutation when compared to wild-type GroEL.

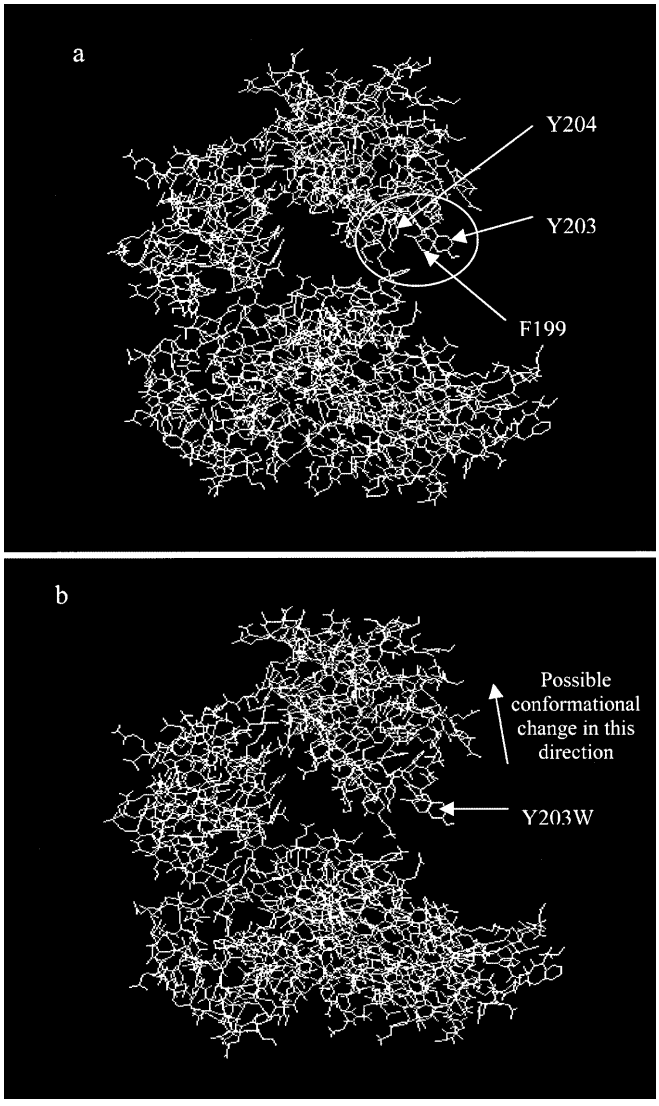

Fig. 1a, b GroEL subunit showing tryptophan mutation is positioned with phenylalanine slightly behind and tyrosine to the side, repositioning of the molecule compared to tyrosine may cause a disruption in the compact 14-mer. **a** Shows the position of the tyrosine at residue numbers 203 and 204 and phenylalanine at residue 199. **b** Shows the tyrosine to tryptophan replacement (Y203W) and indicates the possible disruption that may occur. Both figures were obtained from the Brookhaven databank and modified using RASMOL public domain molecular modelling software

Materials and methods

GroEL preparation

For this study, a GroEL mutant obtained from modified *E. coli* with a single point mutation Y203W was used together with a wild-type GroEL. Preparation of both the GroEL mutant and wild-type GroEL prior to delivery was as described in Gibbons et al. (1996) and Jones et al. (1998), respectively. Both samples were stored as a precipitate in a 75% saturated ammonium sulfate buffer containing 50 mM tetraethylammonium (TEA) (pH 7.5), 50 mM KCl and 20 mM $MgCl_2$.

Prior to use small quantities of the precipitated protein solution were centrifuged at 13,000 rpm for 15 min using a microcentrifuge. The supernatant was then removed and discarded. The protein pellet was resuspended in "Paley" phosphate chloride buffer of pH 7.0, ionic strength $I = 0.1$ mol/l (Green 1933), containing 4.595 g/l $Na_2HPO_4 \cdot 12H_2O$, 1.561 g/l KH_2PO_4 and 2.923 g/l NaCl (Fisher Scientific, Loughborough, UK), typically at 500 µl for every 1 ml of precipitate originally used, and agitated with a 1 ml pipette to resuspend the pelleted protein. Care was taken at this point in order to prevent the formation of bubbles in the solution. Once resuspended the sample was dialysed overnight at 4 °C against 1 l of the same buffer.

The concentration of the dialysed sample was determined by absorption spectroscopy at 280 nm using the Beer-Lambert equation, and an extinction coefficient of 253 ml g^{-1} cm^{-1} for GroEL Y203W and 183 ml g^{-1} cm^{-1} for wild-type GroEL, as calculated from the amino acid compositions (Table 1).

Sedimentation equilibrium analysis

Sedimentation equilibrium was performed using both an Optima XL-I (Beckman Scientific, Palo Alto, USA) analytical ultracentrifuge, equipped with a laser light source and on-line Rayleigh interference optics (Furst 1997), and (for the lowest sample concentration analysed) a Beckman Model E analytical ultracentrifuge, also equipped with a laser light source and interference optics coupled in-house to a purpose built diode array "CCD" camera linked to a Macintosh computer for on-line analysis.

Table 1 Estimated properties of GroEL based on the amino acid sequence at 20 °C

Molecule	Monomer molecular weight (g/mol)	Partial specific volume $\bar{v}$ (ml/g)	Estimated hydration (g/g)	Charge of monomer (Z) at pH 7.0	Experimental charge of 14-mer at pH 7.0[a]	Isoelectric point at pH 7.0	Extinction coefficient (ε_{280}) (ml g^{-1} cm^{-1})
Wild-type GroEL	57,138	0.7377	0.4303	−18.615	−266	5.102	183
GroEL Y203W	57,161	0.7421	0.4298	−18.614	−266	5.100	253

[a] Charge (valency, Z) of the 14-mer determined by Brazil et al. (1998)

Interference optics were favoured over the absorption optical system (also available on the XL-I) since after an initial wavelength scan an optical density at 278 nm of less than 0.1 for a 1 mg/ml GroEL Y203W sample in a 12 mm optical path length cell was obtained. Concentrations were also generally too small for the Schlieren optical system on the Model E to be utilised.

Sedimentation equilibrium using the Beckman Optima XL-I

The low or intermediate speed method (Creeth and Harding 1982) was used. At this speed the concentration at the meniscus remains finite and can be found from mathematical manipulation of the fringe data. Double sector cells of 12 mm optical path length were used with solutions in one sector and dialysate in the other. Solution column lengths of 0.25 cm were employed (corresponding to a loading volume of ~80 µl), with 0.5, 0.7, 1.0, 2.0, 2.35 and 4 mg/ml sample loading concentrations used for GroEL Y203W and 0.3, 0.5, 0.8, 1.0, 1.5, 2.0, 2.5, 3.0 and 3.5 mg/ml loading concentrations used for wild-type GroEL. The loaded ultracentrifuge cells were then placed in a 4-hole titanium rotor, and run at an equilibrium rotor speed of 6000 rev/min. Since sedimentation equilibrium runs take several hours to attain equilibrium (normally performed overnight), a low temperature was used (10 °C) to minimise possible degradative phenomena. Equilibrium was obtained after 20 h, as confirmed by superposition of successive scans taken 2 h apart. These data were then transferred to the MSDOS QUICKBASIC programme MSTARI, which amongst other things evaluates (1) the apparent weight-average molecular weight over the distribution of macromolecular solute in the ultracentrifuge cell (from meniscus to cell base), $M_{w,app}$, and (2) the point or local apparent weight-average (apparent) molecular weights, $M_{w,app}(r)$, as a function of radial position r; (1) is obtained from using an operational point-average molecular weight known as the "star average", M^*, and the identity $M^*(r \to r_b) = M_{w,app}$ (Creeth and Harding 1982), where r_b is the radial position of the cell base, and (2) from sliding strip fits to a plot of ln $J(r)$ versus r^2 (Teller 1973).

Sedimentation equilibrium using the Beckman Model E-II

A further experiment was performed at 0.3 mg/ml for the Y203W sample in the Beckman Model E ultracentrifuge, taking advantage of the larger optical path length ultracentrifuge cells (30 mm) that can be utilised in this instrument, permitting lower concentration measurements.

The conditions and methods used for analysis with the Model E were as described above for the analysis with the XL-I ultracentrifuge except that 250 µl of the 0.3 mg/ml GroEL Y203W sample was needed to give the ~0.25 cm solution column. The cell was then loaded into a rotor (rotor J) and run at 6000 rpm and 10 °C overnight, after which two images were captured 2 h apart to establish that equilibrium had been reached. Data analysis was undertaken using a modification (Walters 2000) of the programme ANALYSER (Rowe et al. 1992) for automatic data capture from the CCD imager. This programme uses a Fourier cosine series algorithm to produce an accurate record of relative fringe displacement $j(r)$ [relative to the fringe displacement J_a at the meniscus (r_a)] versus radial displacement r from the rotor centre. All data were captured and analysed using MSTARI ultracentrifuge data analysis software (Cölfen and Harding 1997).

Sedimentation velocity

All sedimentation velocity experiments were performed in the XL-I ultracentrifuge using Raleigh interference optics. Loading concentrations of 0.3, 0.5, 0.7, 0.8, 1.0 and 1.1 mg/ml loading concentrations were used for GroEL Y203W with 0.3, 0.5, 0.8, 1.0, 1.5 and 2.0 mg/ml loading concentrations were used for wild-type GroEL. The run speed and temperature were set at 40,000 rpm and 20 °C, respectively, throughout with a scan interval of 4 min. All sedimentation coefficients were determined using the latest so-called time derivative [$g^*(s)$ analysis] windows software ("DCDT+", version 1.01) based on Stafford (1992) and provided by Dr. John Philo (Biotechnology & Software Consulting, Thousand Oaks, Calif., USA). All sedimentation coefficients were automatically corrected to standard conditions of 20 °C and water as the solvent ($s_{20,w}$) by DCDT+ using the relation (see, e.g., Tanford 1961):

$$s_{20,w} = s_{T,b}\left(\frac{\eta_{T,b}}{\eta_{20,w}}\right)\left(\frac{1-\bar{v}\rho_{20,w}}{1-\bar{v}\rho_{T,b}}\right) \quad (1)$$

where $\eta_{T,b}$, $\rho_{T,b}$ are the viscosity and densities of the buffer, b, at the temperature, T, of the experiments and $\eta_{20,w}$, $\rho_{20,w}$ the corresponding values for water at a temperature of 20 °C. $s_{20,w}$ values were then extrapolated to "infinite dilution" to eliminate non-ideality effects. The zero concentration value is denoted $s^0_{20,w}$ (see, e.g., Tanford 1961).

GroEL properties from amino acid composition

Some molecular properties based on the amino acid composition were calculated for both the wild-type and Y203W mutant prior to analysis of the ultracentrifuge data. For this the MS Windows routine SEDNTERP (where the user can either enter the amino acid composition data manually or direct from a file) proved useful, based on the paper of Laue et al. (1992). This routine, amongst other things, estimates the monomer molecular weight, M_1, the partial specific volume, $\bar{v}$, the isoelectric pH, the charge (valency), Z, at a specified pH and the extinction coefficient, ε, at 278 nm (Table 1).

The SEDNTERP value relating to Z (the theoretical charge of the monomer) is shown to be very close to experimental values obtained by Brazil et al. (1998), of −266 per 14-mer at pH 7.5, thus leading to a degree of confidence in the theoretical values obtained by SEDNTERP.

Results

Sedimentation velocity analysis

DCDT + analysis of sedimentation velocity data for the Y203W mutant reveals consistently three distinct sedimenting species for sample loading concentrations of 0.3–0.7 mg/ml (Fig. 2) (analysis of the 0.8–1.1 mg/ml loading concentration samples was hindered by the lack of usable XL-I scans and are therefore omitted here), with $s^0_{20,w}$ values of (22.8 ± 0.60) S, (33.5 ± 0.05) S and (39.8 ± 1.09) S (Fig. 3), for the three $g^*(s)$ "peaks" (sedimentating boundaries), respectively. These values are approximately constant throughout the concentration ranges of 0.3–0.7 mg/ml. Figure 3b and Table 3 show the actual concentration values corrected for each sedimenting species, based on the relative amounts of each present. The total relative amount of each sedimenting species, as estimated by taking the peak area as a percentage of the total area of the fitted Gaussian peaks, also remained essentially independent of cell loading concentration, giving mean percentage values of (75.2 ± 1.0)% for the 22.8S component, (18.8 ± 0.5)% for the 33.5S component and (6.0 ± 1.0)% for the 39.8S component (Table 2). This suggests that there is virtually no concentration dependence of the ratio between the three components and hence there is no dynamic equilibrium taking place at the concentration ranges used in these experiments. These results are in stark contrast to those from DCDT + analysis of the native wild-type GroEL protein, which yielded only a single component (Fig. 2b) with an extrapolated $s^0_{20,w}$ value of (21.6 ± 0.3) S (Fig. 3b), which is in excellent agreement with the results of Behlke et al. (1997); there is also a slight positive slope in the $s_{20,w}$ versus c plot, indicative of the presence of a small amount of associative-dissociative equilibria.

Sedimentation equilibrium

Figure 4 shows plots of the apparent (i.e. not corrected for thermodynamic non-ideality) weight-average

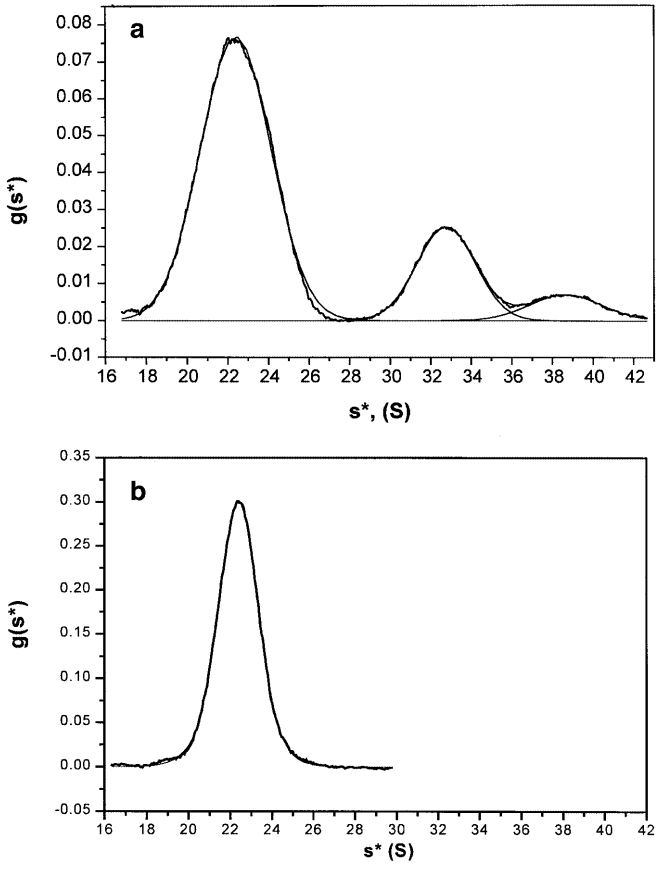

Fig. 2 Apparent distribution of sedimentation coefficients $g^*(s)$ profiles from sedimentation velocity for **a** GroEL Y203W, showing three distinct sedimenting species, and **b** wild-type GroEL showing a single sedimenting species. Both samples were in phosphate-chloride buffer, pH 7.0, $I = 0.1$. Similar profiles were shown throughout the entire concentration ranges used (data not shown). The routine DCDT + was used

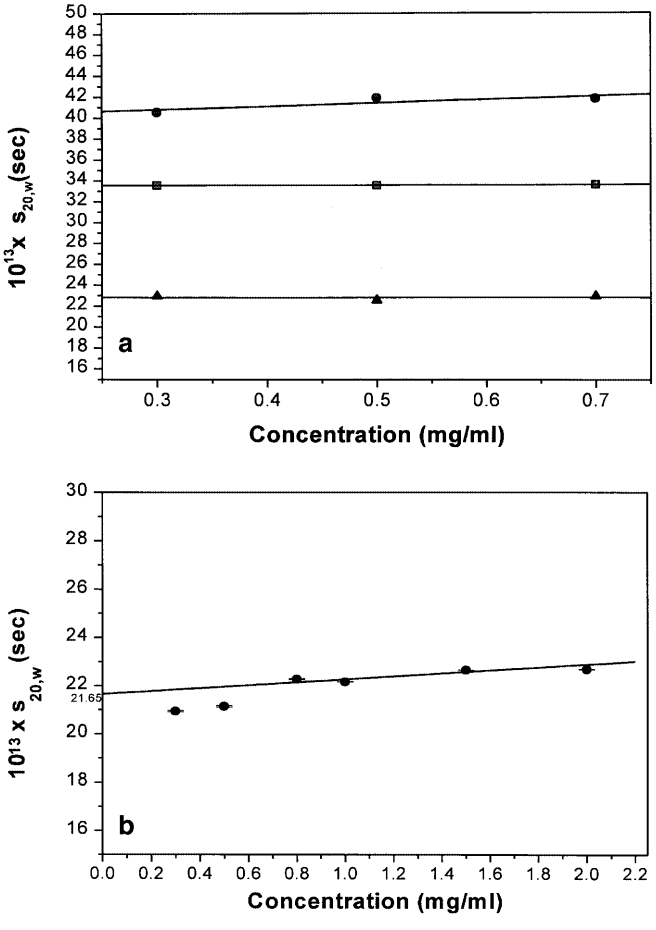

Fig. 3a, b Plots of $s_{20,w}$ versus sedimentation concentrations for each sample (in phosphate-chloride buffer, pH 7.0, $I = 0.1$). **a** Shows $s_{20,w}$ for GroEL Y203W plotted against total protein loading concentration. $s^0_{20,w}$ values for the three sedimenting species are given as ▲ = (22.8 ± 0.60) S, ● = (33.5 ± 0.05) S, ■ = (39.8 ± 1.09) S. **b** Shows $s_{20,w}$ plots verses loading concentration for wild-type GroEL. The $s^0_{20,w}$ value for the single species is given as (21.6 ± 0.3) S

Table 2 Percentage total of each sedimenting species for GroEL Y203W[a]

Concentration (mg/ml)	Gaussian peaks expressed as a percentage of the total area		
	Peak 1	Peak 2	Peak 3
0.3	74.0	19.0	7.0
0.5	76.0	18.5	5.5
0.7	75.5	19.0	5.5
Mean	75.2	18.8	6.0
Standard deviation (σ)	0.9	0.3	0.86

[a] Percentage total of each species was determined as Gausian peak area as a percentage of the total area (Fig. 2)

Table 3 Corrected concentrations of each sedimenting species for GroEL Y203W[a]

Species 1 (mg/ml)	Species 2 (mg/ml)	Species 3 (mg/ml)
0.225	0.057	0.018
0.375	0.095	0.030
0.525	0.133	0.042

[a] Sample concentration was corrected to actual concentrations by taking the percentage total of each sedimenting species (Table 2) as a percentage of the loading concentration

molecular weights ($M_{w,app}$), evaluated from low-speed sedimentation equilibrium versus initial loading concentration: Fig. 4a for the Y203W mutant and Fig. 4b for the native wild-type GroEL. These plots yield extrapolated "ideal" molecular weights, $M_w = M_{w,app}$ ($c \to 0$), of (911,200 ± 54,000) Da for the Y203W mutant and (805,000 ± 5200) Da for the wild-type GroEL molecule, the latter again in excellent agreement with Behlke et al. (1987). The corresponding plots of $1/M_{w,app}$ versus concentration (Fig. 4c and d) were fitted to the equation

$$1/M_{w,app} = (1/M_w)(1 + 2BM_w c) \quad (2)$$

to obtain values for the thermodynamic non-ideality "second virial coefficient" B; values of $\sim 1.8 \times 10^{-5}$ ml mol g^{-2} for the Y203W mutant and $\sim 2.5 \times$

Fig. 4 a Plot of $M_{w,app}$ versus loading concentration, c, for GroEL Y203W (in phosphate-chloride buffer, pH 7.0, $I = 0.1$); an extrapolated M_w ($c \to 0$) gives (911,200 ± 54,000) g/mol. **b** Corresponding reciprocal plot for GroEL Y203W ($1/M_{w,app}$). **c** Wild-type GroEL (in phosphate-chloride buffer, pH 7.0, $I = 0.1$); an extrapolated M_w ($c \to 0$) gives (805,000 ± 5200) g/mol. **d** Corresponding reciprocal plot for wild-type GroEL ($1/M_{w,app}$)

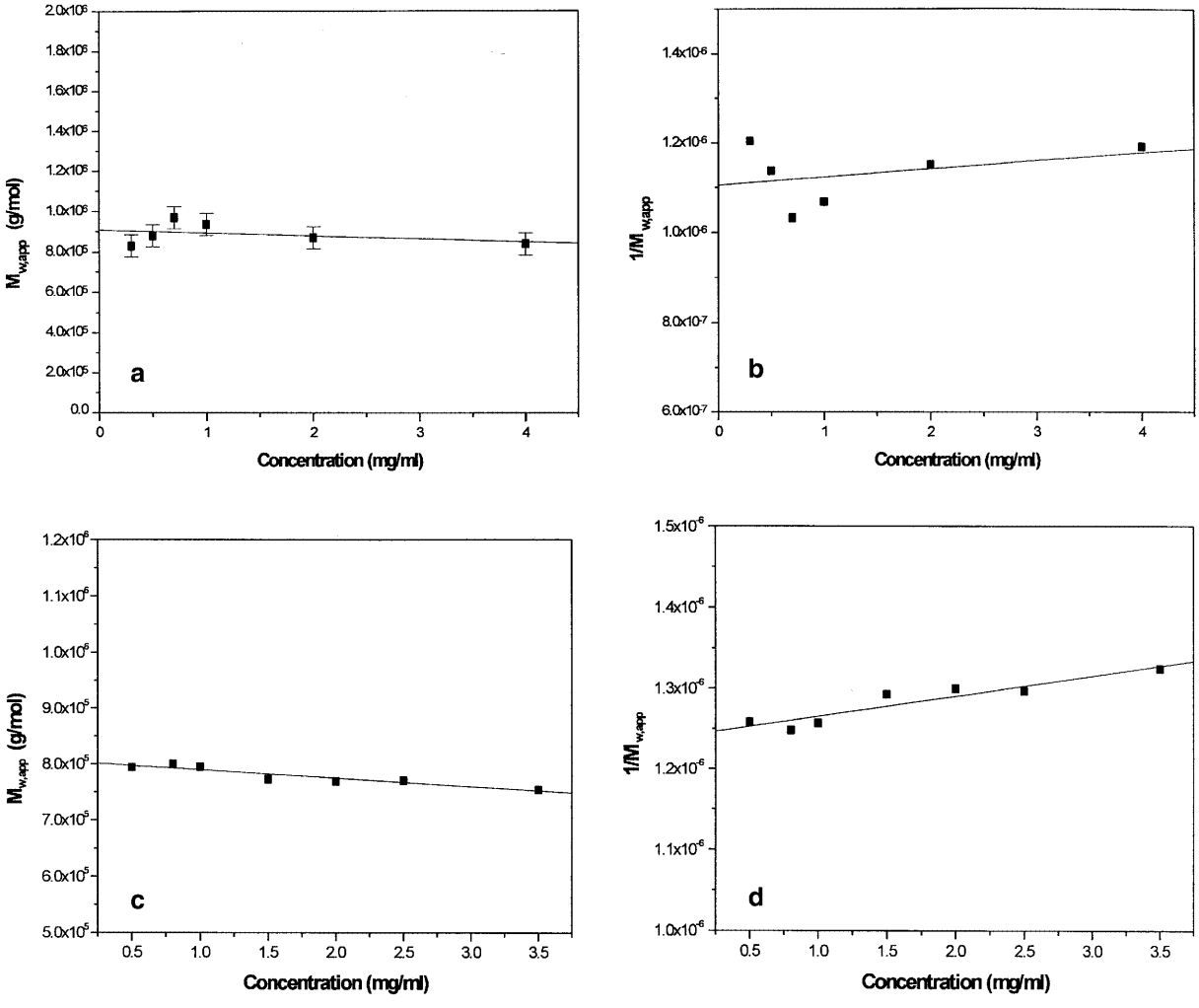

10^{-5} ml mol g^{-2} for wild-type GroEL were respectively obtained.

It is also useful in terms of the stoichiometry to plot point-average molecular weight distribution $M_{w,app}$ (r) verses local (fringe) concentration $J(r)$ in the ultracentrifuge cell as this may give additional information about the distribution of the calculated molecular weights throughout the concentration ranges used (see, e.g., Roark and Yphantis 1969). Figure 5a and b shows such comparisons for a range of different loading concentrations for the Y203W mutant and wild-type GroEL, respectively. To facilitate this comparison, for the Y203W mutant (Fig. 5a) we have normalised the $J(r)$ data for the $c = 0.3$ mg/ml loading concentration data set by a factor of 1/2.5 to allow for the 2.5× larger optical path length (30 mm) cell used. The point-average

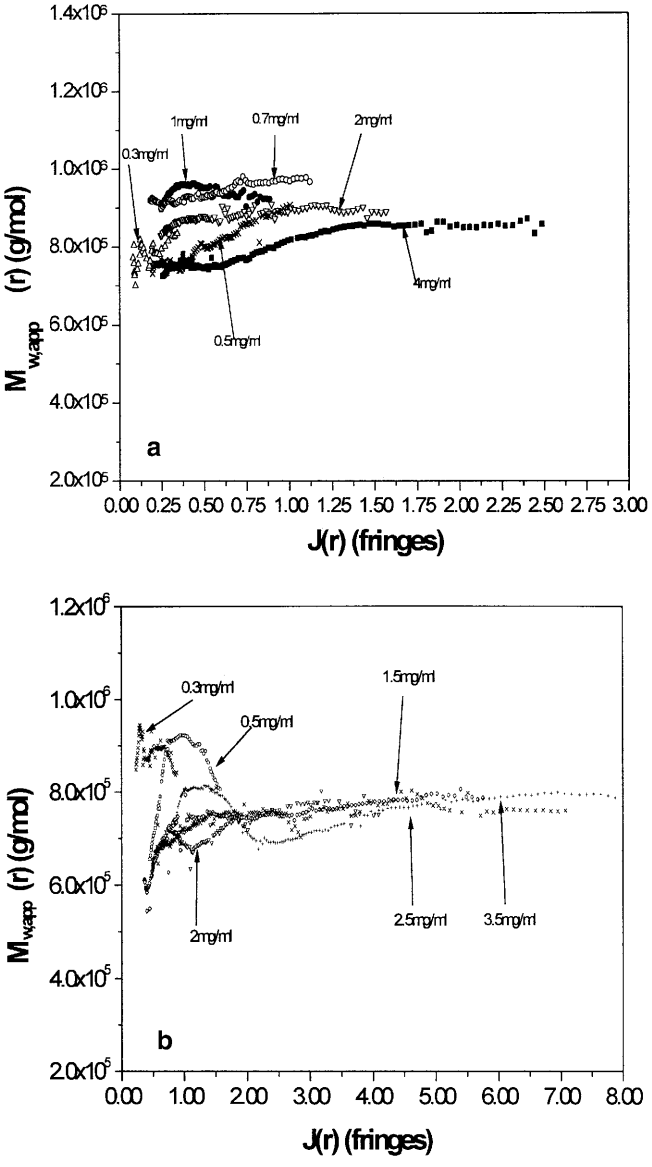

Fig. 5a, b Point-average molecular weights plots of $M_{w,app}(r)$ versus fringe displacement $J(r)$ for different loading concentrations c: **a** GroEL Y203W, 0.3–4 mg/ml, **b** wild-type GroEL, 0.3–3.5 mg/ml

molecular weight plots given for the Y203W mutant reveal an interesting comparison between Y203W and the wild-type in that there is considerably greater superposition of the different data sets at different loading concentrations for the wild-type compared to the Y203W mutant. Non-superposition of data sets is well known to be symptomatic of the presence of different components not in reaction equilibrium with each other (Roark and Yphantis 1969); these data are therefore consistent with the observations from sedimentation velocity that showed the wild-type to be essentially homogeneous whereas the mutant Y203W to have at least three different non-reacting components present. It is also interesting to observe that, despite the unavoidable noise at low concentration (because of the small fringe increments), Fig. 5b does appear to suggest some dissociative behaviour at low concentration; this appears to be reflected also in the $s_{20,w}$ versus c data of Fig. 3b: the extrapolated $s^0_{20,w}$ value of (21.6 ± 0.3) S may be a slight underestimate of the true value for the native 14-mer. Ignoring the first two data points and taking an average of the other four values yields a slightly revised estimate for the $s^0_{20,w}$ value of ~23 S.

Dilute solution conformation

Known sedimentation coefficient ratios (s_n/s_1), which are dependent on the geometry of the molecule, were originally determined for a wide range of oligomeric states and postulated quaternary arrangements in terms of (spherical) bead models by Bloomfield et al. (1967), based on the ratios of frictional coefficients f_n/f_1, where the sedimentation coefficient ratios are obtained from the relationship $s_n/s_1 = n/(f_n/f_1)$. Successive improvements here have been made based on refinements to the hydrodynamic theory of bead models by Garcia Bernal and Garcia de la Torre (1980) and more recently by Carrasco and Garcia de la Torre (1999). According to the latter study, for a dimer of beads $s_2 = 1.436 \times s_1$. Similarly a linear trimer would be $s_3 = 1.743 \times s_1$, whilst for a triangular trimer $s_3 = 1.847 \times s_1$. Using this method, and assuming each GroEL14-mer is approximately spherical, if we take the main 22.8S (~75% by weight) component as corresponding to the 14-mer then the 33.5S species would correspond to a 28-mer (i.e. a linear dimer of 14-mers, which would be predicted as $s_2 = 32.8$S). Similarly, the measured 39.8S species corresponds to a linear trimer of s_1 (predicted s_3 for this model is 39.74S, whereas for a triangular model it would be 42.11S) Fig. 6).

The routine ELLIPS1 (Harding et al. 1997) was also used to estimate the gross conformation of the three sedimenting species shown for Y203W via evaluation of the translational frictional ratio (f/f_0) given by:

$$\left(\frac{f}{f_0}\right) = \left[\frac{M(1-\bar{v}\rho_0)}{N_A(6\pi\eta_0 s^0_{20,w})}\right]\left(\frac{4\pi N_A}{3\bar{v}M}\right)^{1/3} \quad (3)$$

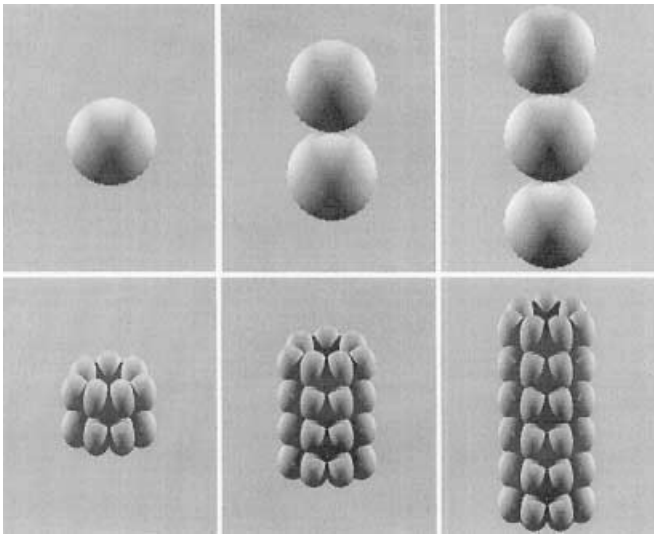

Fig. 6 Simple schematic bead model representation of: **a** GroEL (single sphere) and proposed GroEL dimer (two spheres) and trimer (three spheres) general positioning, and **b** a more detailed view of the proposed 14-mer (monomer), 28-mer (dimer) and 42-mer (trimer) subunit composition. Each monomer unit corresponds to a cpn60 ($M = 60{,}000$ Da) of axial ratio 1.5:1 based on the triaxial ellipsoid originally described by Taylor et al. (1983), using the programs protruder (Hubbard 1994) and SURFNET (Laskowski 1995) and fitted to the crystal structure (Braig et al. 1994). Models were produced using the public domain shareware rendering package Polyray v1.8, provided by Alexander Enzmann (Woburn, USA)

where ρ_0 and η_0 are the density and viscosity of water at 20 °C, $\bar{v}$ is the partial specific volume of the GroEL molecule and N_A is Avogadro's number. For the mutant GroEL we obtained translational frictional ratios values of 1.25, 1.40 and 1.50 for the 22.8S, 33.5S and 39.8S sedimenting species, respectively. In comparison, we obtained a frictional ratio of 1.30 for the wild-type GroEL sample, which is again in excellent agreement with that given by Behlke et al. (1997).

The corresponding Perrin function (P) required for axial ratio determination (of the equivalent prolate ellipsoid) can then be obtained from the relation:

$$P = \left(\frac{f}{f_0}\right)\left[\frac{\delta}{\bar{v}\rho_0} + 1\right]^{-1/3} \quad (4)$$

A value for the "hydration" (δ), needs to be known or estimated; an estimate is possible from the amino acid components, and a value of ~0.43 g/g for both the mutant and wild-type GroEL is obtained. Values for the Perrin function are given as 1.083, 1.175 and 1.290 for the 22.8S, 33.5S and 39.8S species, respectively. Using the routine, ELLIPS 1 (see Harding et al. 1997) for the mutant GroEL the axial ratios (a/b) for each sedimenting species was accordingly given as ~2.5 for the 22.8S species, 4.0 for the 33.5S species and 5.6 for the 39.8S species, which together with the value given for the Perrin function is consistent with the elongation expected with the presence of dimer and trimer conformations. The a/b ratio for the wild-type GroEL is given as 3.0, which is again expected as the proposed conformational change of the mutant GroEL model would predict an outward movement of the apical regions and therefore would have a smaller a/b ratio than the wild type.

Discussion

In this study we have analysed the GroEL Y203W mutant and wild-type GroEL chaperonin from *E. coli* by analytical ultracentrifugation to determine the effects of the tryptophan replacement on the oligomeric integrity of the GroEL molecule. The sedimentation equilibrium results for the Y203W mutant gives an unequivocal demonstration of heterogeneity: for a normal 14-mer of GroEL we would expect a molecular weight of ~800,000 Da (since the monomer, $M_1 \approx 57{,}100$ Da). This corresponds well with the findings from wild-type GroEL analysis, which gives an apparent weight-average molecular weight ($M_{w,app}$) of (805,000 ± 5200) Da (Fig. 4b). However, for the mutant there is clearly species of molecular weight present causing $M_{w,app}(r)$ values in excess of 1 million Da (Fig. 5a). It is clear also that a significant proportion of the species of different molecular weight are not in thermodynamic equilibrium; this is because plots of point average $M_{w,app}(r)$ versus fringe displacement $J(r)$ for different loading concentrations c do not overlap (Fig. 5a); a purely reversibly associating system should give superposition (Roark and Yphantis 1969). This view appears to be strengthened by the results from sedimentation velocity of the GroEL Y203W sample (Fig. 2), where there is also clear heterogeneity from the $g^*(s)$ versus s plots with three discrete sedimenting species present (22.8S, 33.5S and 39.8S), the proportions of which do not change with change in loading concentration (the proportion of the slower moving species should increase with decrease in c if there was a true reversible equilibrium).

We can see that using the sedimentation coefficient values to estimate the multi-subunit conformation of the three discrete species reveals the presence of a monomer, linear dimer and linear trimer conformations for the 22.8S, 33.5S and 39.8S species, respectively. This deduction would appear to be supported by the axial ratio (a/b) determination for prolate ellipsoids using the programme ELLIPS 1, which gave 2.5, 3.8 and 5.6 for the 22.8S, 33.5S and 39.8S sedimenting species, respectively. This is consistent with the elongation expected with the presence of linear dimer and trimer subunit compositions (Fig. 6). In addition, simple analysis of the relative concentrations of the three species which would give an estimated weight-average molecular weight of $(1.0 \pm 0.1) \times 10^6$ Da shows correlation within error of the $M_{w,app}$ of (910,000 ± 50,000) Da, determined directly by sedimentation equilibrium.

No such heterogeneity is observed for unsubstituted wild-type GroEL, which shows a main species of

(21.6 ± 0.3) S which is again in strong agreement with that found by Behlke et al. (1997). These observations may be linked to those of Gibbons et al. (1996), who showed the tryptophan mutation Y203W causes a slight conformational change and hence increased hydrophobic patch exposure in the GroEL molecule; these workers observed that the tryptophan mutant Y203W still retained its ability to fold rhodanese in vitro but was reduced to 30% efficiency compared to 41% for wild-type GroEL (26% reduction) and was also able to interact with substrates including co-chaperonin and nucleotides to assist in protein folding in vivo, thus indicating a non-fatal change in conformation takes place. Possibly the reduction in efficiency is related to the additional presence of the ~25% multi-14-mer species.

The hydrodynamic results of the present study give a clear demonstration of heterogeneity of the Y203W GroEL mutant in the form of monomer (14 subunits), dimer (28 subunits) and trimer (42 subunits) subunit compositions, stressing the importance of the Y203 in both conformational and binding roles of the GroEL molecule. This again shows that a simple amino acid substitution can have a noticeable effect on the conformation and oligomeric state of a protein assembly. The effect of the tryptophan replacement in GroEL may be a reaction to the increased bulk of the Trp. Although perhaps not fully appreciated from the single subunits shown in Fig. 1, this could lead to steric differences and may force surrounding molecules to be repositioned in the compact GroEL 14-mer. In addition, the loss of the tyrosine's reactive hydroxyl group and the less accessible positioning of the indole-based nitrogen of the tryptophan may possibly cause a slight upward movement away from the central cavity (Fig. 1). The tryptophan mutation is positioned with phenylalanine above and tyrosine slightly to the side of it; repositioning of the molecule compared to tyrosine may cause a disruption in any local pi stack that may exist in this position. Although not as dramatic as, say, the valine substitution in haemoglobin associated with sickle cell anaemia, such structural changes do relate to observed changes in conformation and hence the functional performance of such assemblies.

Acknowledgements We thank Dr. Annette Erbse at Birmingham University, UK (now at Yale University, USA) for preparing and supplying the wild-type GroEL. We also thank Dr. Susan Jones at the Biomolecular Structure & Remodelling Unit, University College London, for performing the ellipsoid fit to crystallographic data for cpn60. This work was supported by the award 97/3395 of the UK BBSRC.

References

Behlke J, Ristau O, Schönfeld HJ (1997) Nucleotide dependent complex formation between the *Escherichia coli* chaperonins GroEL and GroES studied under equilibrium conditions. Biochemistry 36: 5149–5156

Bloomfield V, Dalton WO, van Holde KE (1967) Application of the Kirkwood theory to the calculation of frictional coefficients for molecules of various shapes. Biopolymers 5: 135–148

Braig K, Otwinowski Z, Hegde R, Boisvert DC, Joachimiak AL, Sigler PB (1994) The crystal structure of the bacterial chaperonin GroEL at 2.8 Å. Nature 371: 578–586

Brazil BT, Ybarra J, Horowitz PM (1998) Divalent cations can induce the exposure of GroEL hydrophobic surfaces and strengthen GroEL hydrophobic binding interactions. J Biol Chem 273: 3257–3263

Carrasco B, Garcia de la Torre J (1999) Improved hydrodynamic interactions in macromolecular bead models. J Chem Phys 111: 4817–4826

Chen S, Roseman AM, Hunter AS, Wood SP, Burston SG, Ranson NA, Clark AR, Saibil HR (1994) Location and folding protein shape changes in GroEL-GroES complexes images by cryo-electron microscopy. Nature 371: 261–264

Cölfen H, Harding SE (1997) MSTAR and MSTARI: interactive PC algorithms for simple, model independent evaluation of sedimentation equilibrium data. Eur Biophys J 25: 333–346

Creeth SE, Harding SE (1982) Some observations on a new type of point average molecular weight. J Biochem Biophys Methods 7: 25–34

Fenton WA, Kashi Y, Furtak K, Harwich AR (1994) Residues in chaperonin GroEL required for polypeptide binding and release. Nature 371: 614–619

Furst AJ (1997) The XL-I ultracentrifuge with Rayleigh interference optics. Eur Biophys J 25: 307–310

Garcia Bernal JM, Garcia de la Torre M (1981) Transport properties of oligomeric subunit structures. Biopolymers 20: 129–139

Gething MJ, Sambrook J (1992) Protein folding in the cell. Nature 355: 33–45

Gibbons GL, Hixon JD, Hay N, Lund PA, Gorovits BM, Ybarra J, Harowitz PM (1996) Intrinsic fluorescence studies of the chaperonin GroEL containing single Tyr-Trp replacements reveal ligand induced conformation changes. J Biol Chem 271: 31989–31995

Green AA (1933) The preparation of acetate and phosphate buffer solutions of known pH and ionic strength. J Am Chem Soc 55: 2331–2336

Harding SE, Horton JC, Cölfen H (1997) The *ELLIPS* suite of macromolecular conformation algorithms. Eur Biophys J 25: 347–359

Hemmingsen SM, Woolford C, van der Vies SM (1988) Homologous plant and bacterial proteins chaperone oligomeric protein assembly. Nature 333: 330–334

Hubbard S (1994) PROTRUDER: a FORTRAN program to calculate an equi-momental ellipsoid and protrusion index calculations. University College London

Jones S, Wallington EJ, George R, Lund PA (1998) An arginine residue (Arg101) which is conserved in many GroEL homologues, is required for interactions between the two heptameric rings. J Mol Biol 282: 789–800

Langer T, Pfeifer G, Martin J, Baumeister W, Hartl FU (1992) Chaperonin mediated protein folding: GroES binds to one end of the GroEL cylinder, which accommodates the protein substrate within its central cavity. EMBO J 11: 4757–4765

Laue TM, Shah BD, Ridgeway TM, Pelletier SL (1992) Computer-aided interpretation of analytical sedimentation data for proteins. In: Harding SE, Rowe AJ, Horton JC (eds), Analytical ultracentrifugation in biochemistry and polymer science. Royal Society of Chemistry, Cambridge, pp 90–125

Laskowski RA (1995) SURFNET: a program for visualising molecular surfaces, cavities and interactions. J Mol Graphics 13: 323–330

Roark D, Yphantis DA (1969) Studies of self-associating systems by equilibrium ultracentrifugation. Ann NY Acad Sci 164: 245–278

Rowe AJ, Wynne Jones S, Thomas DG, Harding SE (1992) Methods for off-line analysis of sedimentation velocity and sedimentation equilibrium patterns. In: Harding SE, rowe AJ, Horton JC (eds) Analytical ultracentrifugation in biochemistry

and polymer science. Royal Society of Chemistry, Cambridge, pp 49–62
Saibil HR (1994) How chaperonins tell right from wrong. Nat Struct Biol. 1: 838–842
Saibil HR, Zheng D, Roseman AM, Hunter AS, Watson GMF, Chen S, auf der Mauer A, O'Hara BP, Wood SP, Mann NH, Barnett LK, Ellis RJ (1993) ATP induces large quaternary rearrangements in cage like chaperonin structure. Curr Biol 3: 265–273
Stafford WF III (1992) Sedimentation boundary analysis in sedimentation transport experiments: a procedure for obtaining sedimentation coefficient distributions using the time derivative of the concentration profile. Anal Biochem 203: 295–301
Tanford C (1961) Sedimentation in the ultracentrifuge. In: Physical chemistry of macromolecules. Wiley, New York, pp 364–390
Taylor WR, Thornton JM, Turnell RJ (1983) An ellipsoidal approximation of protein shape. J Mol Graph 1: 30–38
Teller DC (1973) Characterisation of proteins by sedimentation equilibrium in the analytical ultracentrifuge. Methods Enzymol 27: 346–441
Walters C (2000) PhD dissertation (in preparation)